Title
Effects of Heterogeneity and Friction on the Deformation and Strength of Rock

Authors
Nihei, K.T.
Myer, L.R.
Kemeny, J.M.
et al.

Publication Date
1994-03-15

LBL-35457
UC-400

Lawrence Berkeley Laboratory
UNIVERSITY OF CALIFORNIA

EARTH SCIENCES DIVISION

To be presented at the Europe–U.S. Workshop on Fracture and Damage in Quasibrittle Structures: Experiment, Modeling and Computer Analysis, Prague, Czech Republic, September 21–23, 1994, and to be published in the Proceedings

Effects of Heterogeneity and Friction on the Deformation and Strength of Rock

K.T. Nihei, L.R. Myer, J.M. Kemeny, Z. Liu, and N.G.W. Cook

March 1994

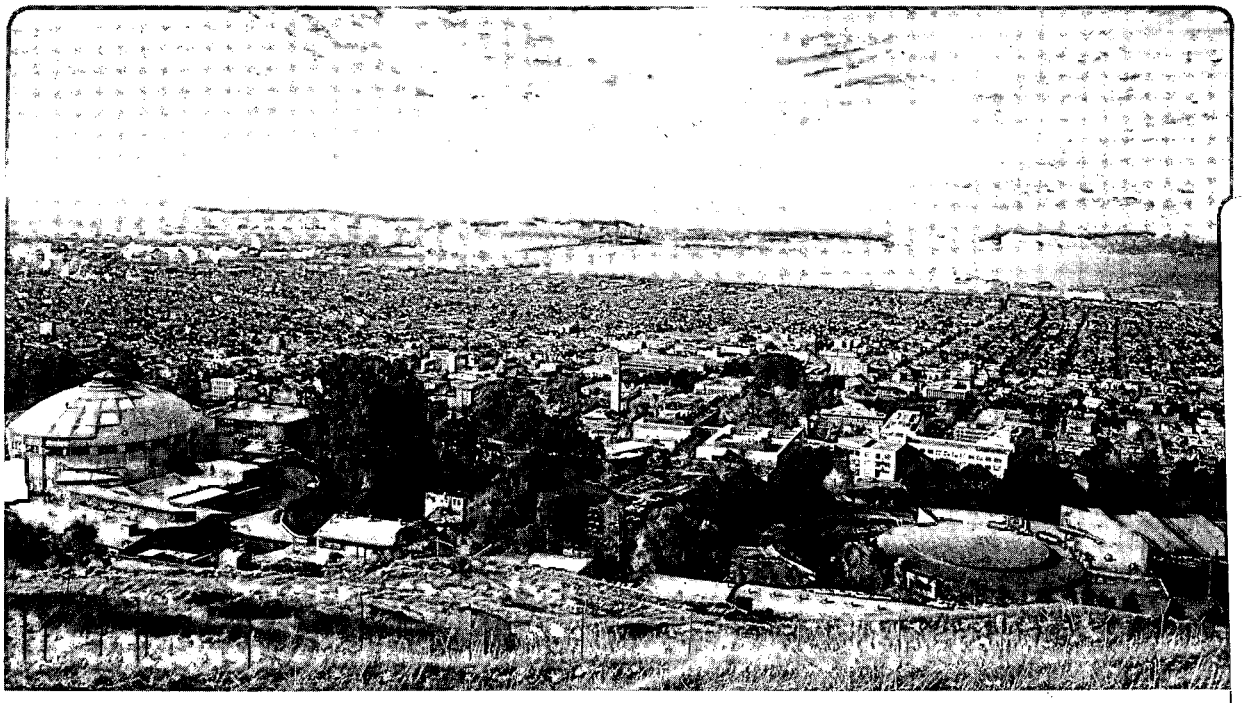

Prepared for the U.S. Department of Energy under Contract Number DE-AC03-76SF00098

DISCLAIMER

LBL-35457
UC-400

Effects of Heterogeneity and Friction on the Deformation and Strength of Rock

K.T. Nihei and L.R. Myer

Earth Sciences Division
Lawrence Berkeley Laboratory
University of California
Berkeley, California 94720

J.M. Kemeny

Department of Mineralogy and Geological Engineering
University of Arizona
Tucson, Arizona

Z. Liu and N.G.W. Cook

Department of Materials Science and Mineral Engineering
University of California
and
Earth Sciences Division
Lawrence Berkeley Laboratory
University of California
Berkeley, California 94720

March 1994

This work was supported by the Director, Office of Energy Research, Office of Basic Energy Sciences, Engineering and Geosciences Division of the U.S. Department of Energy under Contract No. DE-AC03-76SF00098. Work performed at the University of Arizona was supported by the National Science Foundation Solid and Geomechanics Program under Grant No. MSS9022381 and by Cyprus Mining Company.

Effects of Heterogeneity and Friction on the Deformation and Strength of Rock

K.T. NIHEI and L.R. MYER
Earth Sci. Div., Lawrence Berkeley Laboratory, Berkeley, California, USA
J.M. KEMENY
Dept. of Min. & Geo. Engin., University of Arizona, Tucson, Arizona, USA
Z. LIU and N.G.W. COOK[1]
Dept. of Mat. Sci. & Min. Engin., University of California, Berkeley, California, USA

Abstract

Experimental observations of the evolution of damage in rocks during compressive loading indicate that macroscopic failure occurs predominantly by extensile crack growth parallel or subparallel to the maximum principal stress. Extensile microcracks initiate at grain boundaries and open pores by a variety of micromechanical processes which may include grain bending, Brazilian type fracture and grain boundary sliding. Microstructural heterogeneity in grain size, strength and shape determines the magnitude of the local tensile stresses which produce extensile microcracking and the stability with which these microcracks coalesce to form macrocracks. Friction at grain boundaries and between the surfaces of microcracks reduces the strain energy available for extensile crack growth and increases the stability of microcrack growth. In clastic rocks, frictional forces may improve the conditions for extensile microcrack growth by constraining the amount of sliding and rotation of individual grains.

Micromechanical models are used to investigate the effects of heterogeneity and friction on the deformation and strength of crystalline and clastic rocks. Models based on the periodic and random assemblages of sliding cracks are capable of replicating many aspects of the nonlinear stress-strain behavior of rocks but do not predict interaction of en echelon extensile microcracks which leads to shear localization. Numerical micromechanical models based on the boundary element method have been developed to investigate the effects of microstructural heterogeneity and friction on the initiation, coalescence and localization of extensile microcracks in crystalline and clastic rocks. These models demonstrate that the stochastic arrangement and properties of microcracks in a crystalline rock and grains in a clastic rock can have a first order effect on the deformation and strength characteristics.

1 Introduction

In response to differential compressive stresses, most rocks exhibit complex patterns of strain. Initially, the slope of the stress-strain curve increases, as low aspect ratio microcracks and imperfect grain boundaries close. This non-linear deformation is succeeded by a near-linear stress-strain behavior, often interpreted as elastic deformation, although frictional sliding occurs between microcrack surfaces resulting in hysteresis between the loading and unloading portions of the stress-strain curve. Before the peak of the stress-strain curve, microcrack growth in the direction of the maximum applied stress results in strain-hardening and dilatation. Deformations greater than those corresponding to the peak strength of the

[1]also at Earth Sci. Div., Lawrence Berkeley Laboratory, Berkeley, California, USA.

rock usually follow strain-softening and for small applied confining stresses, are accompanied by extreme dilatation produced by extensile microcracks. Higher confining stresses tend to suppress dilatation and, in clastic rocks, result in pore collapse as grains undergo comminution and compaction [1] [2].

It is important to recognize how this complex non-linear stress-strain behavior is influenced by the microstructure of the rock. The stochastic arrangement of grain boundaries, pores and microcracks in rock produce local concentrations of tensile stress, even when the rock is subjected only to compressive stresses, that result in extensile microcracking. The extensile microcracks, predominantly aligned parallel to the maximum principal stress axis, produce dilatation and stress-induced elastic anisotropy, as observed by [3]. It is likely that the growth and coalescence of these extensile microcracks is also controlled by the stochastic distribution of microcrack lengths and orientations in crystalline rocks and the stochastic distribution of grain sizes, shapes, and elastic properties in clastic rocks. The universal presence of friction between the closed portions of cracks and grain boundaries is also likely to have a first order effect on the overall deformation, strength and stability of rocks. This paper examines the role of microstructural heterogeneity and friction on the deformation and strength of rocks through laboratory observations and numerical micromechanical models.

2 Extensile Microcrack Growth Under Differential Compression

Understanding the influence of microcrack growth began with efforts to account for the strength of rock using a Griffith approach (e.g., [4]). Subsequently, the influence of microcracks on the effective moduli of rocks was analyzed by Walsh [5] [6]. The effects of microcracks on elastic moduli and strength in the strain-softening part of the stress-strain curve was analyzed by Cook [7] and others. A key concept was the recognition that heterogeneities in the microstructure produce local concentrations of tensile stress, even when the rock as a whole is subjected to compressive stresses. These local tensile stresses generate extensile microcracks that are aligned in the direction of the maximum principal stress and produce dilatation.

Experimental observations of microcrack growth under differential compression have been made by Wawersik and Brace [8], Hallbauer et al. [9], Kranz [10], Batzle et al. [11], Fredrich and Wong [12], Myer et al. [13], and others. These observations confirmed that mode I extensile microcracking occurs parallel to the direction of the maximum compressive stress and that there are several mechanisms responsible for the local tensile stress concentrations. Studies of crack growth in glass and plastic [14] led to the development of the *sliding crack* model (e.g., [15]) in which mode II deformation on cracks inclined to the maximum compressive stress direction produce growth of mode I *extensile wing cracks* that ultimately run parallel to the direction of the maximum compressive stress. Recent experimental work on clastic rocks has shown that extensile microcracking is not limited to test conditions in which the stress conditions are nearly uniform, such as in a compression test in a cylindrical sample, but also occurs in a variety of loading conditions such as those found around a cylindrical borehole and beneath an indenter [13].

In the absence of confining stress, interaction between the microcracks causes macrofractures that take the form of extensile splitting cracks, which grow parallel to the direction of the maximum compressive stress and form adjacent to the traction-free surfaces. Confining stress introduces a compressive stress at the ends of extensile microcracks which inhibits the extension of the longest cracks while allowing shorter cracks to nucleate and

grow. Unconfined compression, therefore, produces a lower density of longer extensile microcracks while confined compression produces a more uniform population of shorter microcracks. For confining stresses approaching the uniaxial compressive strength, shear bands composed of en-echelon arrays of extensile microcracks form, coalescing into a macroscopic shear fracture. In clastic rocks, higher confining stresses results in grain crushing and pore collapse which is characterized by a near linear relation between porosity reduction and the cumulative number of acoustic emission events [1]. Porosity reduction and yielding is enhanced for non-hydrostatic loading where local shear stresses produce frictional sliding and grain rotation, leading to the enhanced compaction of the pore space [2].

Direct observations of the microstructure of clastic rocks as it exists under load can be obtained using a Wood's metal porosimetry technique [13]. In this technique, compression tests are performed at approximately 100°C with a molten Wood's metal (Cerrosafe® alloy; melting point ≈ 88°C) as the pore fluid. At the stress-state of interest, the temperature is reduced to room temperature to solidify the Wood's metal. The Wood's metal filling the open pore space, grain boundaries and cracks preserves the microstructure as it existed under load and provides a high contrast material in SEM (scanning electron microscope) backscatter photomicrographs for visualizing microcracks. Preserving the microstructure under load avoids the problem of crack closure, which was found by Zhao et al. [16] to reduce the total number of visible cracks by as much as fifty percent.

Using the Wood's metal technique, Zheng et al. [17] observed that the dominant micromechanical process associated with failure of Indiana limestone under unconfined conditions is the growth of long extensile cracks. Tests conducted at various stages of failure were observed to be consistent with the model that divides the process of extensile crack formation and growth into four stages: nucleation of microcracks, unstable growth of the nucleated crack for some distance dependent on the stress conditions, stable growth, and interaction of cracks leading to unstable growth. Visual examination at higher SEM magnifications [13] revealed a number of mechanisms of extensile crack formation which include grain bending [18], pore squeezing [19], Hertzian contact point loading [1], Brazilian test compressive loading, and combined point loading and bending.

3 Frictional Sliding on Grain Boundaries and Microcracks

Friction is an important, but often overlooked, micromechanism which contributes significantly to the overall deformation and strength of both crystalline and clastic rocks. It is likely that the processes of frictional sliding and lock-up on previously existing grain boundaries and microcracks and stress induced microcracks play a major role in determining the strength and failure characteristics of rocks.

Direct evidence for the presence of friction in rocks is the observed hysteresis between the loading and unloading portions of the stress-strain curve. Walsh [6] and Cook and Hodgson [20] recognized that the disparity between the tangent moduli computed from the loading and unloading portions of the stress-strain curve results from frictional sliding along grain boundaries and closed microcracks during loading that *lock-up* on initial unloading and do not reverse slide until the load is reduced to a value where the locked in local compressive stresses are sufficient to initiate reverse sliding. Cook and Hodgson postulated that the tangent moduli computed from small unloading excursions where friction is locked-up are equivalent to those computed from the velocities of small strain (i.e., $\varepsilon < 10^{-6}$) seismic waves. Fig. 1 displays $\sigma - \varepsilon$ measurements on dry Berea sandstone from Hilbert et al. [21] for uniaxial strain loading. Concurrent ultrasonic P- and S-wave velocity measurements

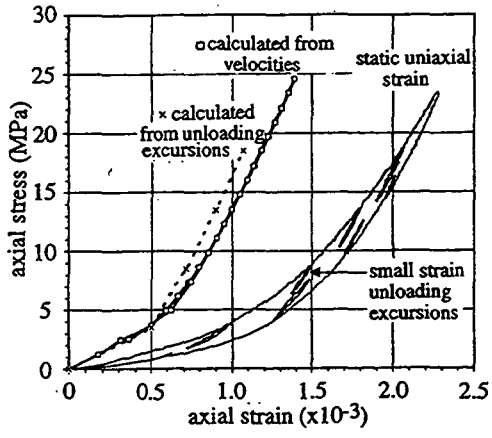

Fig. 1. An experimental axial stress-strain curve for dry Berea sandstone under uniaxial strain showing small-amplitude unloading cycles together with curves derived from the integration of small-strain elastic moduli derived from unloading cycles and seismic velocities.

made during the test were converted into moduli then integrated to determine a stress-strain curve. Because the dynamic strains of the ultrasonic waves are too small to cause significant frictional sliding [22], the dynamic $\sigma-\varepsilon$ curve is equivalent to the static $\sigma-\varepsilon$ curve without the effects of friction. To verify this, strains measured from the small unloading excursions of the static $\sigma-\varepsilon$ curve were integrated to reconstruct a second static $\sigma-\varepsilon$ curve without the effects of friction. The similarity between the $\sigma-\varepsilon$ curves computed from the ultrasonic velocities and the static unloading excursions indicates that the difference between elastic moduli computed from elastic wave velocities and from the slope of the tangent to the static $\sigma-\varepsilon$ curve is caused by the difference in the strain amplitudes associated with the two measurement techniques and not by the difference in loading rates. One practical implication of this result is that crack density calculations based on elastic wave velocities may grossly underestimate crack densities since small strain elastic waves do not probe closed microcracks which, nevertheless, may contribute significantly to the large strain deformation of the rock through frictional sliding.

During the nucleation and growth of cracks, frictional sliding along favorably oriented grain boundaries and closed cracks constitute crack-closing tractions that resist crack displacements, thereby, reducing the energy available for extensile microcrack growth and effectively stabilizing the system. Similar frictional stabilization effects have been recognized as a toughening mechanism in brittle ceramics [23]. The magnitude of this effect is likely to be large given the amount of hysteresis typically observed during the failure of a rock, but has yet to be quantified. In porous rocks loaded with moderate confining stresses, frictional sliding plays a significant role in the process of shear-enhanced compaction which is a combination of particle crushing followed by readjustment of the subparticles by sliding and rotation. In the post-failure (localization) regime, strength and deformation characteristics of rocks are thought to be controlled by sliding along several well developed macrocracks [7] [3]. While it is clear from this discussion that there is sufficient evidence to postulate that friction across grain boundaries, microcracks and macrocracks influences the overall deformation and strength of rocks, additional theoretical work is needed.

4 Micromechanical Modeling

Because of the basic similarity in rock deformation and failure under compression in a wide variety of rock types , it is not surprising that the various micromechanical failure processes in crystalline and clastic rocks have many similarities [24]. Kemeny and Cook [25] have demonstrated that the various micromechanical models for extensile microcrack growth (e.g., sliding crack, pore squeezing, point loading, dislocation pile-up, grain bending, etc.) share the following similarities:

1. Crack growth occurs predominantly in the σ_1 direction.
2. K_I proportional to a size parameter, such as pore or grain size, initial crack length, etc.
3. Unstable growth occurs initially when the crack length is close to the size parameter.
4. Stable crack growth occurs when the crack length is much larger than the size parameter.
5. K_I decreases rapidly with increasing σ_2.
6. K_I is linearly proportional to $\sigma_1 - C\sigma_2$, where C is a constant.
7. Non-interacting microcracks produce only strain-hardening and crack interaction is required to produce strain-softening.

These similarities may explain the success of certain micromechanical models, such as the sliding crack model, in spite of the lack of evidence for these models in laboratory studies.

4.1 Nonlinear Rock Deformation Due to Crack Growth, Interaction, and Coalescence

The nonlinear stress-strain behavior of a body containing cracks is illustrated conceptually in Fig. 2a. In the absence of crack growth, the stress-strain behavior is linear. As load is increased, extensile cracks will begin to grow when the applied stresses are sufficient to generate a strain energy release rate, G, equal to the crack resistance, G_c, of the rock, as indicated by point A in Fig. 2a. The cracks on which this criterion is satisfied are allowed to grow an increment in length, and the new effective modulus, $\overline{M}_i$, of the cracked rock is computed from the strain energy of the crack, U^c, using Castigliano's theorem,

$$\varepsilon_i^c = \frac{\partial U^c}{\partial \sigma_i} = \frac{\partial}{\partial \sigma_i}\left\{2\int_0^l G\, dl\right\} \rightarrow \overline{M}_i = \frac{\sigma_i}{(\varepsilon_i^c + \varepsilon_i^o)} , \tag{1}$$

where l is the new crack length, σ_i is the applied principal stress, and ε_i^c and ε_i^o are the principal strains of the crack and the intact material, respectively.

Initially, crack growth is stable since the stress must be continually increased to sustain crack growth and increase deformation. Macroscopically, this process results in strain-hardening behavior, as illustrated by the path from A to B, and the new effective modulus reflects the increase in strain energy associated with crack growth. As stress is increased above that of state B, crack interaction will occur. As cracks begin to interact, the condition may arise in which cracks will continue to grow even under decreasing stress. This leads to macroscopic strain-softening behavior of state C. This also results in lower effective moduli which reflect the presence of longer cracks. As cracks grow and interact, the stress at which $G = G_c$ changes forming a locus of points defining the stress-strain curve, as illustrated in Fig. 2a. This approach for modeling the nonlinear behavior of rock is an inherently stable approach because the nonlinear system is decomposed into a piecewise linear system with a

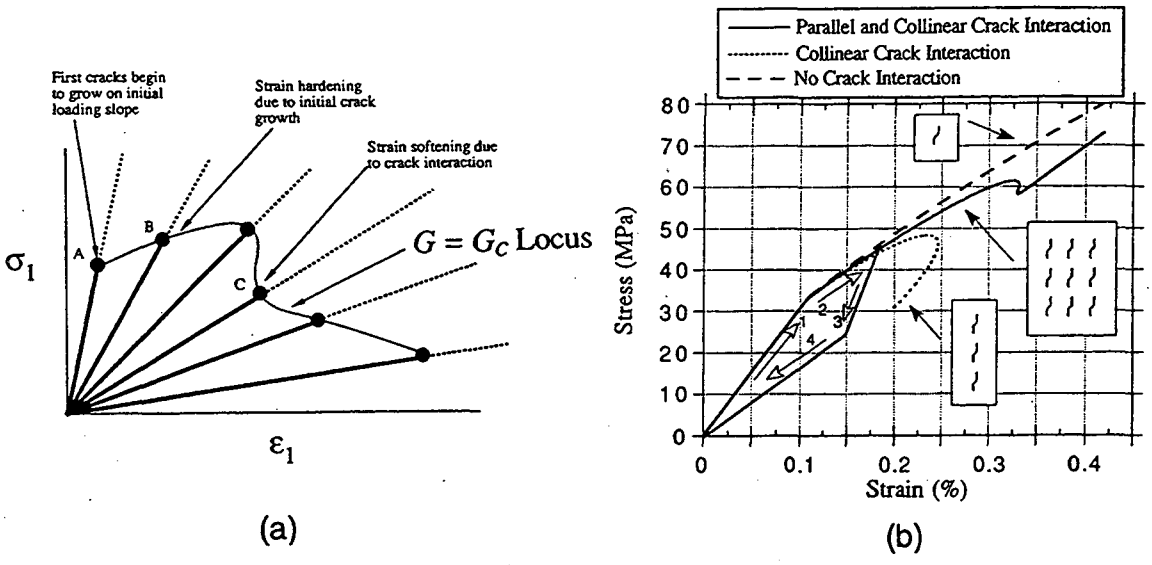

Fig. 2. (a) Sketch showing how a non-linear stress-strain curve can be derived from the effective moduli of a cracked elastic solid and the critical value of stress for each modulus at which crack extension begins. (b) Stress-strain curves for sliding crack models with various degrees of interaction between the cracks.

unique stress-strain relation. This approach has been used in sliding crack models [13] and the two numerical models described in the following sections.

An example of this approach for modeling nonlinear stress-strain curves is displayed in Fig. 2b. The progressive failure of Indiana limestone is simulated using an array of sliding cracks which can close and slide under compressive load. For those cracks that meet the criteria for frictional sliding, tension develops near the tips of the cracks, resulting in the formation of a pair of tensile wing cracks as the loading is increased. Initially the stress-strain curve is linear due to the linear deformation of the elastic material and the sliding along the initial cracks (labeled 1). At a stress of about 35 MPa, crack growth starts to occur. For the model with no crack interaction, only strain-hardening is predicted past this point (labeled 2). For the model that considers collinear crack interaction, strain-hardening followed by unstable (class II) strain-softening is predicted. For the model that considers both parallel and collinear crack interaction, a more complex pattern is predicted in which the unstable strain-softening is stabilized by the parallel crack interaction. Fig.2b also shows the effect of unloading in the sliding crack model. As soon as unloading is initiated, the sliding portions of the cracks will lock up, resulting in initial unloading with a slope corresponding to the intrinsic modulus of the rock (labeled 3). At some value of load, the surfaces of the closed cracks become unlocked, and the rock unloads at a much steeper slope (labeled 4).

4.2 Boundary Element Model for Crystalline Rocks

A limitation of micromechanical models based on periodic assemblages of sliding cracks is their inability to model interactions of randomly distributed and oriented microcracks which may lead to the formation of localized shear bands and ultimately results in macroscopic faulting, as observed in experiments with confinement. The numerical model described in this section considers the deformation of an elastic material containing a random initial distribution of cracks. As load is applied, the cracks will grow, interact, and coalesce, resulting in nonlinear rock behavior and the formation of macroscopic fractures and faults.

This model is a good representation for the heterogeneous behavior of most crystalline rocks in the low-temperature and low-confinement regime. The basis for the model is the displacement-discontinuity boundary element numerical solution of Crouch and Starfield [26] for the static stress field of an elastic continuum permeated with fully interacting cracks. Several modifications to the model, such as the introduction of a modified crack tip element were introduced by Du and Kemeny [27] to improve the accuracy of the computed stress intensity factor.

The basic framework for modeling nonlinear deformation and failure consists of incremental loading or displacement of the rock followed by a stress calculation for the entire crack system to determine if closed cracks will slide and if suitably oriented cracks will grow. Coulomb friction along the closed portions of cracks was implemented using an iterative scheme as described below. First, an initial calculation is made to estimate the shear and normal stresses induced along the cracks due to the problem boundary conditions and geometry without crack interaction. For this initial calculation, the crack surfaces are locked using the boundary conditions $u^s = u^n = 0$, where the superscripts s and n denote shear and normal displacement, respectively. Next, an initial determination is made whether slip will occur along the crack segments. If the normal stress for a crack segment is compressive, then the segment will slip if $|\sigma_i^s| \geq |\sigma_i^f|$, where $\sigma_i^f = c_i - (\sigma_i^n)\tan\phi_i$ and σ_i^f, σ_i^s, σ_i^n, c_i, and ϕ_i are the frictional stress, shear stress, normal stress, cohesion, and friction angle for crack segment i, respectively. If this equation is satisfied, then the boundary conditions $u^n = 0$ and $\sigma_i^s = \sigma_i^f$ are applied to crack segment i. If the computed normal stress on crack segment i is tensile, then the boundary conditions $\sigma_i^n = \sigma_i^s = 0$ are applied. This step is repeated, resulting in an accurate calculation of the frictional forces along each closed crack segment. These iterations are performed along with any crack growth which may occur.

The strain energy density criterion is used to determine the onset of crack growth and the direction of crack growth for each crack tip. The strain energy factor, S, is given by [28]:

$$S = A_{11} K_I^2 + A_{12} K_I K_{II} + A_{22} K_{II}^2 , \tag{2}$$

where

$$A_{11} = \frac{1}{16G}[((3-4\upsilon)-\cos(\theta))(1+\cos(\theta))] \tag{3}$$

$$A_{12} = \frac{1}{16G}[-(1-2\upsilon)+\cos(\theta)]2\sin(\theta) \tag{4}$$

$$A_{22} = \frac{1}{16G}[4(1-\upsilon)(1-\cos(\theta))+(1+\cos(\theta))(3\cos(\theta)-1)] , \tag{5}$$

and where G is the shear modulus and θ is the crack initiation angle. Note that S is a function of K_I and K_{II} which can be calculated using the modified stress intensity factors given in [27]. Crack growth will occur when $S > S_{cr}$, where S_{cr} is a material property determined from laboratory tests. The crack will grow in the direction for which S is minimum. Mathematically, more than one minimum may occur due to the fact that the minimum value of S can occur for both a compressional and tensional tangential stress around the crack tip. The correct minimum will minimize S and also correspond to a tensional stress. Crack extension is performed by adding a new crack tip element of a specified length each time the crack growth criteria is met.

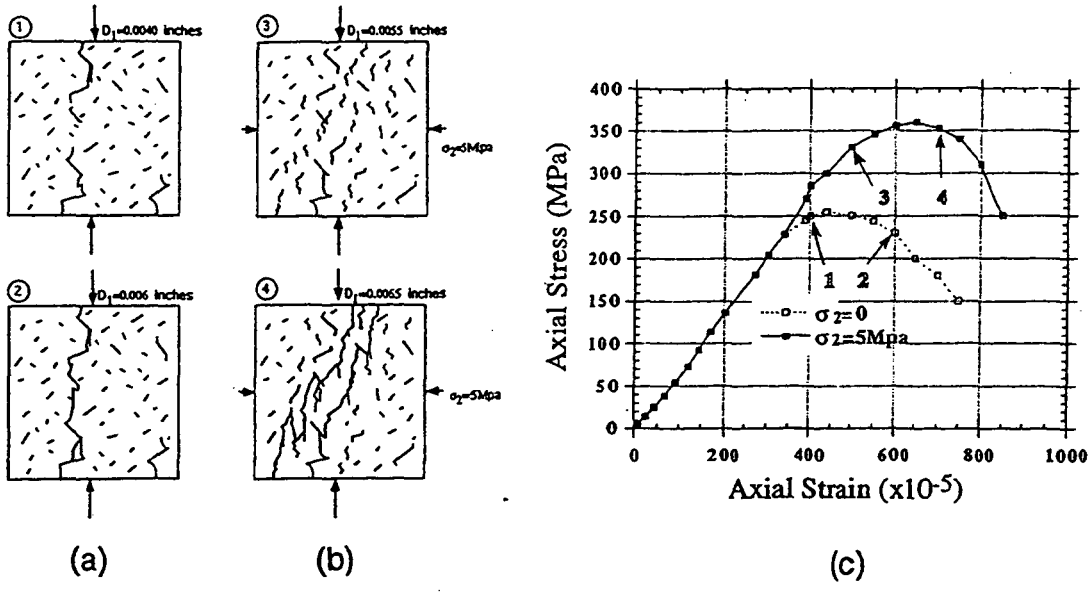

Fig. 3. Numerical results obtained from the boundary element crack model for a random distribution of cracks: (a) uniaxial compression test, (b) confined compression test, and (c) axial stress-strain curves for both tests.

Simulation of compressive failure with and without confinement are displayed in Fig. 3 for stochastic microcrack properties (orientations, lengths, locations) representative of Westerly granite [27]. The crack density and friction coefficient for these simulations are 0.01 and 0.4, respectively. These simulations clearly demonstrate that the introduction of stochastic microcrack properties has two important effects which are not observed in any of the collinear sliding crack models. First, it leads to a transition from axial splitting under uniaxial compression to macroscopic shear fracture under confined compression (Fig. 3), as is commonly observed in the laboratory. Second, it results in significantly larger amounts of non-linear strain-hardening and strain-softening behavior.

4.3 Boundary Element Model for Clastic Rocks

Until recently, most of the work in micromechanical modeling of compressive failure in rock has been based on the idealization of the rock microstructure as an elastic continuum with a population of random or aligned cracks. This particular model is a good abstraction of the true microstructure of many crystalline rocks but may not adequately capture the basic microstructural details of clastic rocks, which contain both grain boundaries and equant porosity. The microstructure of most clastic rocks are more amenable to discrete particle modeling in which individual grains are treated as discrete elastic bodies which interact with neighboring grains through a finite grain contact area. Recently, there has been an explosion in the development of discrete particle modeling methods for investigating deformation, fracture and particle flows in clastic and granular materials [29].

To investigate the role of microstructural heterogeneity on failure in brittle clastic rocks, a discrete particle numerical model has been developed which combines the boundary element method with an efficient substructuring procedure [30]. This model is capable of an accurate determination of the intragranular stresses, unlike most other discrete element models, many of which were concerned mainly with modeling the behavior of soil (e.g., [31] [32] [33]). An accurate estimate of the intragranular stresses is important in modeling the failure of brittle

clastic rocks in which extensile failure of a grain is determined by the local tensile stress concentrations.

The surfaces of each grain are discretized into boundary elements. Neighboring grains are connected together by allowing the displacements and tractions to be continuous across the boundary elements in contact. The boundary integral equation for a single grain written in matrix form is

$$\begin{pmatrix}[f_{11}] & [f_{12}]\\ [f_{21}] & [f_{22}]\end{pmatrix}\begin{pmatrix}\{u_c\}\\ \{u_f\}\end{pmatrix}=\begin{pmatrix}[g_{11}] & [g_{12}]\\ [g_{21}] & [g_{22}]\end{pmatrix}\begin{pmatrix}\{t_c\}\\ \{t_f\}\end{pmatrix}, \tag{6}$$

where f are the coefficients involving the Green's stress tensor, g are coefficients involving the Green's function, u is the boundary displacement, t is the boundary traction, and the subscripts c and f denote parts of the grain associated with the contact and with the traction-free parts of the grain, respectively. The fact that $\{t_f\}=0$ can be used to rewrite or substructure Eq. (6) purely in terms of the unknown contact displacements and tractions,

$$A\{u_c\}=B\{t_c\}, \tag{7}$$

where $A=[f_{11}]-[f_{12}][f_{22}]^{-1}[f_{21}]$ and $B=[g_{11}]-[f_{12}][f_{22}]^{-1}[g_{21}]$.

The straightforward construction of the global system of equations of a packing of n grains would require solving a linear system composed of n equations of form of Eq. (7). This would be extremely computationally intensive for more than a few grains since each grain (i.e., Eq. (7)) is typically discretized into one hundred boundary elements. A more efficient approach is to recognize that the strain energy of the granular packing is transmitted entirely through the grain contacts (since $\{t_f\}=0$) and to exploit this fact by constructing the global system of equations using the Principle of Minimum Energy, as in the Finite Element Method. The total potential energy of the system including the applied tractions, $\{T\}$, is

$$\begin{aligned}\Pi &= 1/2\sum_{i=1}^{n}(\{t\}_i\{u\}_i-\{T\}_i\{u\}_i)\\ &= 1/2\sum_{i=1}^{n}(\{t_c\}_i\{u_c\}_i-\{T\}_i\{u_c\}_i)=1/2\sum_{i=1}^{n}(B_i^{-1}A_i\{u_c\}_i^2-\{T\}_i\{u_c\}_i).\end{aligned} \tag{8}$$

Minimization of the total potential energy of the grain packing results in the following global equation which has been reduced to only the unknown contact displacements,

$$\frac{\partial\Pi}{\partial\{u_c\}_i}=0 \;\rightarrow \sum_{i=1}^{n}(B_i^{-1}A_i\{u_c\}_i-0.5\{T\}_i)=0\,. \tag{9}$$

This approach allows us to accurately model more than 500 grains, as shown in Fig. 4.

To model failure, the grain packing is loaded along the boundaries of the sample in steps and the local tensile stresses are computed at the centers and contact points of every grain in the packing. Failure occurs by extensile fracture of the grain when (σ_1 - Cσ_2) exceeds the tensile strength of the grain or by debonding of the contact when the contact stress exceeds the tensile strength of the bond. When extensile grain failure occurs, the Young's modulus of the grain is reduced and the Poisson's ratio is increased to simulate the effective properties

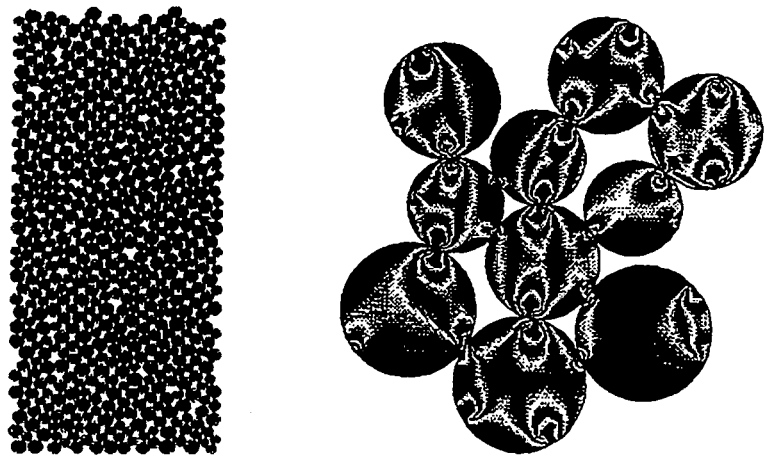

Fig. 4. Distribution of the maximum principal compressive stresses inside a granular packing computed using the boundary element particle model. Note that the stress fields inside each grain can be seen clearly on the enlargement of a few grains (right) and that the same stress fields on the coarse scale give the appearance of columnar trajectories carrying most of the applied load (left).

of a fractured grain. This simplified failure criteria is used instead of explicitly fracturing the grain to avoid remeshing problems which would greatly reduce computational efficiency and limit the number of grains that could be modeled. After a grain failure or contact debonding, the system is unloaded and reloaded to determine the new effective moduli and strength of the grain packing. This iterative procedure obviates any numerical instabilities and enables us to trace out the complete stress-strain curve which may include both strain-hardening and softening.

Using the numerical formalism described above, we have investigated failure in a hexagonal packing of cylindrical grains and found that a uniform strength produces strain-softening and localization while a stochastic strength distribution produces strain-hardening followed by strain-softening and a lower compressive strength [30]. These numerical simulations also exhibited higher compressive strengths for a narrow stochastic distribution of tensile grain strengths and lower compressive strengths for a wide distribution. An important conclusion of this study was that granular materials with homogeneous or narrow stochastic strength distributions display only macroscopic strain-softening and a localized macroscopic shear fracture, while a granular material with a heterogeneous distribution of strengths exhibits both strain-hardening and strain-softening and a more distributed pattern of failure. Similar observations were noted by Lawn et al. [23] who found that microstructural heterogeneity, induced in initially homogeneous brittle ceramics, transformed these materials from brittle to *effectively ductile*.

The effects of heterogeneity in the grain size on the stress-strain behavior of a random grain packing with identical grain strengths is shown in Fig. 5 for uniaxial and biaxial compression. Each line in the plot corresponds to reloading of the system after a grain has either failed in tension or by debonding of a grain contact. The effective modulus is reduced as damage progresses, as indicated by the lower slopes of these lines. The dotted line, which traces out an envelope of the effective moduli lines each terminated at the stress which causes microscopic fracture, is the macroscopic stress-strain curve. This curve exhibits both strain-hardening and strain-softening behavior. Application of confining stress, stabilizes the

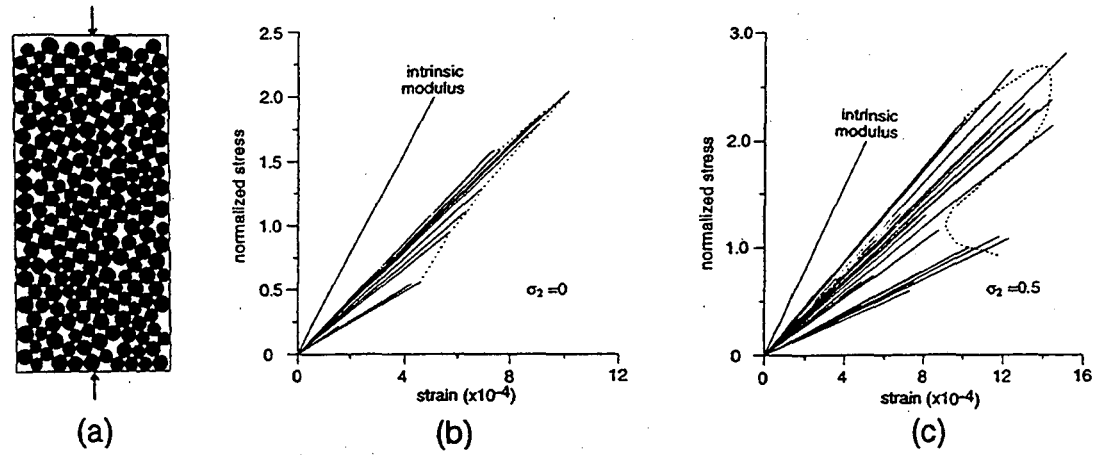

Fig. 5. (a) Grain packing with a uniform stochastic distribution of particle sizes (radius= 0.9 to 1.1), (b) axial stress-strain curve for uniaxial compression test dominated by strain-softening, and (c) axial stress-strain curve for biaxial compression test exhibiting both strain-hardening followed by strain-softening. Stresses are normalized by the tensile strength of the grains.

system, as indicated by the increased peak stress and the greater amount of strain-hardening.

At present, the model is limited to infinitesimal displacements and does not include the effects of intergranular frictional sliding, finite displacements and rotations, and grain fragmentation. Incorporation of these additional phenomena into numerical micromechanical models are essential for a complete understanding of deformation and failure of clastic rocks, particularly when confining stresses are sufficiently large to induce grain comminution and finite sliding and rotation. We are presently developing a discrete particle model with improved contact mechanics [34] and grain fracture capabilities.

5 Conclusions

Observation has shown that the heterogeneous microstructure of most rocks results in local tensile stress concentrations with magnitudes large enough to cause mode I extensile microcracking even when the applied stresses are compressive. While the initial growth may be unstable, continued extension of isolated cracks is stable and occurs in a direction near parallel to the direction of the maximum applied compressive stress. Microcrack growth prior to interaction with neighboring microcracks results in strain-hardening dilatant deformation. As the differential stress is increased, cracks begin to interact, resulting in strain-softening dilatant deformation. Interaction between cracks leads to macroscopic splitting cracks in unconfined compression. Confining stresses suppress the growth of long, isolated extensile cracks so that interaction tends to produce shear bands composed of en echelon arrays of cracks.

Frictional sliding at grain boundaries and between the surfaces of microcracks reduces the strain energy available for extensile crack growth and increasing the stability of microcrack growth. In clastic rocks, frictional forces may improve the conditions for extensile microcrack growth by constraining the amount of sliding and rotation of individual grains. Friction also plays a major role in the deformation of rock in the strain-softening region where deformation is observed to occur by sliding along developed macrocracks. Further research in this area is warranted to quantify these observations.

Insight into the mechanics of nonlinear deformation and strength of rocks can be obtained using the concepts linear elastic fracture mechanics. The generic behavior of extensile

fracture models justifies the use of the simple sliding crack model, even though it is not the dominant extensile failure mechanism observed in most rocks. Periodic arrays of sliding cracks with row and column interactions reproduce much of the observed stress-strain behavior at low confining stresses including strain-hardening due to initial stable crack growth, strain-softening due to crack interaction, and the increase in compressive strength with increasing confining stress due to the stabilization of crack growth.

Analytic solutions based on periodic arrays of sliding cracks capture a good deal of the deformation and strength characteristics of rocks, but these models do not predict the formation of shear localization at higher confining stresses. Boundary element models have been developed to investigate the effects of heterogeneity in the microstructure of crystalline and clastic rocks. The boundary element crack model for crystalline rocks includes frictional sliding along closed cracks and employs a strain energy crack growth criteria. Numerical simulations display strain-hardening and strain-softening behavior and for uniaxial and biaxial loading, exhibits axial splitting and shear localization, respectively. The boundary element model for a clastic rock models deformation due to extensile grain failure and tensile grain contact debonding. Numerical simulations show that heterogeneity in grain strength and grain size control the failure characteristics of clastic rocks.

Acknowledgments

This work was supported by the Director, Office of Energy Research, Office of Basic Energy Sciences, Engineering and Geosciences Division of the US Department of Energy under Contract No. DE-AC03-76SF00098. Work performed at the University of Arizona was supported by the National Science Foundation Solid and Geomechanics Program under Grant No. MSS9022381 and by Cyprus Mining Company.

6 References

1. Zhang, J., Wong, T.-F. and Davis, D.M. (1990a) Micromechanics of pressure-induced grain crushing in porous rocks, *Journal of Geophysical Research*, Vol.95, No.B1, 341-352.
2. Zhang, J., Wong, T.-F., Yanagidani, T. and Davis, D.M. (1990b) Pressure-induced microcracking and grain crushing in Berea and Boise sandstones: acoustic emission and quantitative microscopy measurements, *Mechanics of Materials*, Vol.9, 1-15.
3. Brace, W.F. (1971) Micromechanics of rock systems, in Structure, *Solid Mechanics and Engineering Design*, (ed. M. Te'eni), Wiley-Interscience, London, 187-204.
4. McClintock, F.A. and Walsh, J.B. (1962) Friction on Griffith cracks in rocks under pressure, *Proceedings of the 4th US National Congress on Applied Mechanics*, Vol.2, ASME, New York, 1015-1021.
5. Walsh, J.B. (1965a) The effect of cracks on the compressibility of rock, *Journal of Geophysical Research*, Vol.70, No.2, 381-398.
6. Walsh, J.B. (1965b) The effect of cracks on the uniaxial elastic compression of rocks, *Journal of Geophysical Research*, Vol.70, No.2, 399-411.
7. Cook, N.G.W. (1965) The failure of rock, *International Journal of Rock Mechanics & Mineral Science*, Vol.2, 389-403.
8. Wawersik, W.R. and Brace, W.F. (1971) Post-failure behavior of a granite and diabase, *Rock Mechanics*, Vol.3, 61-85.
9. Hallbauer, D.K., Wagner, H. and Cook, N.G.W. (1973) Some observations concerning the microscopic and mechanical behavior of quartzite specimens in stiff,

triaxial compression tests, *International Journal of Rock Mechanics & Mineral Science*, Vol.10, 713-726.

10. Kranz, R.L. (1980) The effect of confining pressure and stress difference on the static fatigue of granite, *Journal of Geophysical Research*, Vol. 85, 1854-1866.
11. Batzle, M.L., Simmons, G. and Siegried, R.W. (1980) Microcrack closure in rock under stress: direct observation, *Journal of Geophysical Research*, Vol.85, 7072-.
12. Fredrich, J.T. and Wong, T.-F. (1989) Micromechanics of thermally induced cracking in three crustal rocks, *Journal of Geophysical Research*, Vol.91, 12743-12764.
13. Myer, L.R., Kemeny, J.M., Zheng, Z., Suárez-Rivera, R., Ewy, R.T. and Cook, N.G.W. (1992) Extensile cracking in porous rock under differential compressive stress, in *Micromechanical Modelling of Quasi-Brittle Material Behavior*, (ed. V.C. Li), *Applied Mechanics Reviews*, Vol.45, No.8, ASME, 263-280.
14. Brace, W.F. and Bombolakis, E.G. (1963) A note on brittle crack growth in compression, *Journal of Geophysical Research*, Vol.68, 3709-3713.
15. Nemat-Nasser, S. and Horii, H. (1982) Compression-induced nonplanar crack extension with application to splitting,.exfoliation, and rock burst, *Journal of Geophysical Research*, Vol.87, 6805-6822.
16. Zhao, Y., Huang, J. and Wang, R. (1993) Real-time SEM observations of the microfracturing process in rock during compression test, *International Journal of Rock Mechanics, Mineral Science & Geomechanics Abstracts*, Vol.30, No.6, 643-652.
17. Zheng, Z., Myer, L.R. and Cook, N.G.W. (1989) Microcrack geometry in confined and unconfined conditions, *Proceedings of the 30th US Rock Mechanics Symposium*, 749-756.
18. Gallagher, J.J., Friedman, M., Handin, J. and Sowers, G.M. (1974) Experimental studies relating to microfracture in sandstone, *Tectonophysics*, Vol.21, 203-247.
19. Sammis, C.G. and Ashby, M.G. (1986) The failure of brittle porous solids under compressive stress states, *Acta Metall*, Vol.34, 511-526.
20. Cook, N.G.W. and Hodgson, K. (1965) Some details stress-strain curves for rock, *Journal of Geophysical Research*, Vol.70, No.12, 2883-2888.
21. Hilbert, L.B. Jr., Hwong, T.K., Cook, N.G.W., Nihei, K.T. and Myer, L.R. (1990) Effects of strain amplitude on the static and dynamic nonlinear deformation of Berea sandstone, to appear in *Proceedings of the 1st North American Rock Mechanics Symposium*.
22. Mavko, G.M. (1979) Frictional attenuation: an inherent amplitude dependence, *Geophysics*, Vol.84, 4769-4775.
23. Lawn, B.R., Padture, N.P., Cai, H. and Guiberteau, F. (1994) Making ceramics ductile, *Science*, Vol.263, 1114-1116.
24. Horii, H. and Nemat-Nasser, S. (1985) Compression-induced microcrack growth in brittle solids: axial splitting and shear failure, *Journal of Geophysical Research*, Vol.90, 3105-3125.
25. Kemeny, J.M. and Cook, N.G.W. (1991) Micromechanisms of deformation in rocks, in *Toughening Mechanisms in Quasi-Brittle Materials*, (ed. S.P. Shaw), Kluwer Academic, Netherlands, 155-188.
26. Crouch, S.L. and Starfield, A.M. (1983) *Boundary Element Methods in Solid Mechanics*, George Allen & Unwin, London.
27. Du, W. and Kemeny, J.M. (1993) Modeling borehole breakout by mixed mode crack growth, interaction, and coalescence, *International Journal of Rock Mechanics, Mineral Science & Geomechanics Abstracts*, Vol.30, No.7, 809-812.

28. Sih, G.C. (1974) Strain energy density factor applied to mixed mode crack problems, *International Journal of Fracture*, Vol.10, 305-321.
29. Special Issue on Mechanics of Granular Materials (1993) *Mechanics of Materials*, (ed. S. Nemat-Nasser), Vol.16, No.2.
30. Liu, Z., Myer, L.R. and Cook, N.G.W. (1993) Micromechanics of granular materials-numerical simulation of the effects of heterogeneities, *International Journal of Rock Mechanics, Mineral Science & Geomechanics Abstracts*, Vol.30, No.7, 1281-1284.
31. Cundall, P.A. and Strack, O.D.L. (1979) A discrete numerical model for granular assemblies, *Géotechnique*, Vol.29, 47-65.
32. Bruno, M.S. and R.B. Nelson (1991) Microstructural analysis of the inelastic behavior of sedimentary rock, *Mechanics of Materials*, Vol.12, 95-118.
33. Rothenberg, L. and R.J. Bathurst (1992) Effects of particle shape on micromechanical behavior of granular materials, *Advances in Micromechanics of Granular Materials*, (ed. H.H. Shen), Elsevier Science Publishers, Netherlands, 343-352.
34. Hilbert, L.B. Jr., Yi, W., Cook, N.G.W., Cai, Y. and G.-P. Liang (1994) A new discontinuous finite element method for interaction of many deformable bodies in geomechanics, to appear in *Proceedings of the 8th International Conference of the International Association for Computer Methods and Advances in Geomechanics.*

LAWRENCE BERKELEY LABORATORY
UNIVERSITY OF CALIFORNIA
TECHNICAL INFORMATION DEPARTMENT
BERKELEY, CALIFORNIA 94720